

High-pressure behavior of space group $P2/n$ omphacite

FRANCESCO PANDOLFO,^{1,*} FABRIZIO NESTOLA,² FERNANDO CÁMARA,³ AND M. CHIARA DOMENEGHETTI¹

¹Dipartimento di Scienze della Terra e dell'Ambiente, Università di Pavia, via Ferrata 1, I-27100 Pavia, Italy

²Dipartimento di Geoscienze, Università di Padova, via Gradenigo 6, I-35131 Padova, Italy

³Dipartimento di Scienze Mineralogiche e Petrologiche, Università degli Studi di Torino, via Valperga Caluso 25, I-10125 Torino, Italy

ABSTRACT

A single-crystal X-ray diffraction (XRD) study, using a diamond-anvil cell at high pressure and room temperature, was performed on a crystal from a natural space group $P2/n$ omphacite sample with composition very close to $Jd_{55}Di_{45}$ and with a high degree of order in cation distribution. Unit-cell parameters were determined at 13 different pressures up to about 7.5 GPa. A third-order Birch-Murnaghan equation of state (BM3-EoS) fitted to the P - V data yielded $V_0 = 421.43(4) \text{ \AA}^3$, $K_{T0} = 122(1) \text{ GPa}$, and $K' = 5.1(3)$. The K_{T0} value for this sample lies between the data obtained for the two end-members jadeite and diopside, and describes a slight positive curvature trend.

During the same experiment, intensity data were collected and crystal structures were refined at 5 pressures up to 7.3 GPa. Both M1 and M2 polyhedra volumes showed a slight but significant change in slope at about 4 GPa. This behavior can likely be explained in terms of tilt angle variation of TA and TB tetrahedral, which also showed a change in slope with pressure, rather than in terms of bond length compression anomaly.

Keywords: Pyroxene, omphacite, high pressure, single-crystal XRD, crystal structures, diamond-anvil cell, equation of state

INTRODUCTION

Many recent X-ray diffraction studies have focused on the behavior under high-pressure conditions of clinopyroxene with different compositions (Downs 2003; Origlieri et al. 2003; Thompson et al. 2005; Bindi et al. 2006; McCarty et al. 2008; Nestola et al. 2005, 2006, 2007, 2008a, 2010; Gavrilenko et al. 2010). This is likely due to the very wide range of geological high-pressure environments in which this mineral is found, from metamorphic rocks to meteorites, and also as inclusions in diamonds (e.g., Nestola et al. 2007; Koch-Müller et al. 2004). In particular, clinopyroxenes are very abundant in the upper mantle, and most mineralogical and geophysical investigations have concentrated on shedding light on the extremely complex geodynamic processes occurring at that depth (e.g., Agee 1999). Knowledge of the compressional and thermal behavior of clinopyroxenes is fundamental for understanding the geological environments in which these silicates play a crucial role. Concerning the high-pressure behavior of Na-clinopyroxene, X-ray diffraction studies have been performed both on jadeite, aegirine, and hedenbergite end-members and on jadeite-aegirine and jadeite-hedenbergite solid solutions (Nestola et al. 2006, 2007, 2008a).

The compressional behavior of omphacite (solid solution between $\text{CaMgSi}_2\text{O}_6$, $\text{Di-NaAlSi}_2\text{O}_6$, Jd , end-members) was investigated for the disordered phase with space group $C2/c$ by McCormick et al. (1989) by single-crystal X-ray diffraction and by Nishihara et al. (2003) using an in situ multi-anvil apparatus by X-ray synchrotron radiation. The ordered phase with space group $P2/n$, was studied by Pavese et al. (2001) on powder material by X-ray synchrotron radiation. However no studies on the

structural behavior at high pressure have been performed thus far on this mineral. The aim of this work is to define for the first time the crystal-structure evolution as a function of pressure and the pressure–volume equation of state for a natural ordered omphacite of space group $P2/n$ with low-Fe content by single-crystal X-ray diffraction (SCXRD). This work is part of a wider project focused on the high-pressure and high-temperature behavior of natural and synthetic Na-bearing pyroxenes.

EXPERIMENTAL METHODS

Sample

The sample investigated at high pressure in this work comes from the same crystal suite studied by Boffa Ballaran et al. (1998) and is labeled as their sample 74AM33. The chemical analysis of this sample is reported in Table 1. The sample was selected for its very low-Fe content to avoid the effect of iron on the Di-Jd solid solution. This sample also presents the highest degree of order for a natural omphacite among the samples studied by Boffa Ballaran et al. (1998). From this sample we picked out a single crystal, labeled N.4, suitable for the high-pressure experiments due to its sharp optical extinction, sharp diffraction profiles, absence of twinning and evident defects and appropriate crystal size ($0.17 \times 0.12 \times 0.05 \text{ mm}$).

Chemistry

Chemical analysis was performed on the same crystal used for the high-pressure work. After extracting the crystal from the diamond-anvil cell (DAC) it was embedded in epoxy resin and polished for electron microprobe analysis (EMPA), which was carried out at the Dipartimento di Geoscienze (University of Padova) using a CAMECA-CAMEBAX electron microprobe operating in wavelength-dispersive mode with a fine-focused beam ($\sim 1 \mu\text{m}$ diameter), an acceleration voltage of 20 kV and a beam current of 10 nA, with 10 s counting times for both peak and total background. X-ray counts were converted to oxide wt% using the PAP correction program supplied by CAMECA (Pouchou and Pichoir 1991). Standards, spectral lines, and analytical crystals used were: albite ($\text{NaK}\alpha$, TAP), wollastonite (Si, $\text{CaK}\alpha$, TAP), olivine ($\text{MgK}\alpha$, TAP), Al_2O_3 ($\text{AlK}\alpha$, TAP), MnTiO_3 ($\text{MnK}\alpha$, LiF; $\text{TiK}\alpha$, PET), Cr_2O_3 ($\text{CrK}\alpha$, LiF), Fe_2O_3 ($\text{FeK}\alpha$, LiF). The oxide wt% obtained by averaging 15 microprobe analyses are reported in Table 1.

* E-mail: francesco.pandolfo@unipv.it

TABLE 1. Electron microprobe analysis and formula in atoms per formula unit (apfu) based on six oxygen atoms for omphacite crystal N.4 (average of 15 spots)

% oxides		apfu	
SiO ₂	56.1(4)	Si	1.968(7)
TiO ₂	0.11(2)	Al ^{IV}	0.032(7)
Al ₂ O ₃	13.1(2)	Al ^{VI}	0.510(9)
Cr ₂ O ₃	0.03(3)	Fe ³⁺	0.002(3)
FeO	2.33(6)	Fe ²⁺	0.067(4)
MnO	0.03(2)	Mg	0.448(8)
MgO	8.6(1)	Mn	0.0009(6)
CaO	13.0(2)	Ti	0.0030(6)
Na ₂ O	6.9(2)	Cr	0.0009(9)
K ₂ O	0.004(5)	Ca	0.490(7)
Total	100.3(5)	Na	0.47(1)
		K	0.0002(2)
		Total	3.99(1)

Single-crystal X-ray diffraction: Crystal in air

The intensity data collected from the crystal in air were obtained at the University of Pavia on a three-circle Bruker AXS SMART APEX diffractometer, equipped with a CCD detector (graphite-monochromatized MoK α radiation $\lambda = 0.71073$ Å, 55 kV, 30 mA) and a monocarp collimator. The Bruker SMART software package was used. A total of 3360 frames (frame resolution 512×512 pixels) were collected with four different goniometer settings using the ω -scan mode (scan width: 0.2° ; exposure time: 10 s; detector sample distance 4.02 cm). A total of 10337 reflections were collected. Completeness of the measured data was achieved up to $78^\circ 2\theta$. The Bruker SAINT+ software was used for data reduction, including intensity integration and background and Lorentz-Polarization corrections. The semi-empirical absorption correction of Blessing (1995), based on the determination of transmission factors for equivalent reflections, was applied using the program SADABS (Sheldrick 1996) and the monoclinic Laue group $2/m$. The intensity data were refined in space group $P2_1/n$ using the program SHELX-97 (Sheldrick 2008) starting from the atom coordinates by (Pavese et al. 2000). Scattering curves were taken from the *International Tables for X-ray Crystallography* (Wilson 1995). Neutral vs. ionized scattering factors were used to refine occupancy for all sites that are not involved in chemical substitutions (O and Si) (Hawthorne et al. 1995) and ionized scattering factors were used for cationic sites. When the refinement reached convergence, full-matrix least-squares were carried out using the data from the electron microprobe analysis (with 1σ error) as chemical constraints to obtain the site partitioning. The following restraints were introduced into the refinement: (1) all structural sites were considered fully occupied; (2) Al³⁺ was distributed between T, M11, and M1; (3) Mn²⁺ was ordered in M1 while Cr and Ti were considered ordered in M11; (4) Fe²⁺ and Mg were considered as present in both M1 and M11, while Fe²⁺ only in M2 and Mg in M21; (5) charge balance was ensured by the equation $X_{Na}^{M2} + X_{Na}^{M21} = X_{Al^{3+}}^T + X_{Al^{3+}}^{M11} + X_{Al^{3+}}^{M1} + 2X_{Ti} + X_{Cr}$; (6) additional equations based on the $\langle M1-O \rangle$ and $\langle M11-O \rangle$ observed mean bond distances were used to better constrain the site partitioning of Mg and Al in M1 and M11 sites. These equations are $\langle M1-O \rangle = 2.077Mg_{M1} + 1.928Al_{M1} + 2.130Fe_{M1}^{2+} + 2.173Mn_{M1}$ and $\langle M11-O \rangle = 2.077Mg_{M11} + 1.928Al_{M11} + 2.130Fe_{M11}^{2+} + 1.990Ti_{M11} + 2.01Cr_{M11}$. The values of mean bond distances for Mg, Al, and Fe²⁺ are from Boffa Ballaran et al. (1998), values for Mn, Ti, and Cr are from

Zema et al. (1997). The crystal-chemical formula obtained with this procedure is $(Ca_{0.253}Na_{0.737}Fe_{0.010})^{M2}(Ca_{0.713}Na_{0.231}Mg_{0.056})^{M21}(Mg_{0.837}Fe_{0.092}Al_{0.069}Mn_{0.002})^{M1}(Mg_{0.016}Fe_{0.020}Al_{0.957}Ti_{0.006}Cr_{0.001})^{M11}(Al_{0.036}Si_{1.964})^TO_6$. The composition of our sample expressed in end-member mol% is: Jd₄₈Di₄₀Hd₃En₃CaTs₃Fs₁. To compare our data with jadeite and diopside end-members, hereafter we will refer to a composition Jd₅₅Di₄₅, obtained by renormalizing the end-member composition to 100% of Jd-Di. The mean atomic numbers calculated for the octahedral sites [$m.a.n_{M1+M11+M2+M21}$] by EMPA [28.87(13)] and by SCXRD [28.74(31)] are in agreement within their errors. The unit-cell parameters for the crystal in air are reported in Table 2, whereas the values of the conventional agreement factor $R1$ as well as other details from the chemical constrained structure refinement are reported in Table 3. The site populations obtained from this refinement are reported in Table 4, fractional coordinates and displacement parameters in Table 5, and bond lengths and angles in Table 6. The full structural data have also been deposited as CIF¹.

Single-crystal high-pressure X-ray diffraction

The high-pressure SCXRD experiments were carried out at the Dipartimento di Geoscienze, Università di Padova. Crystal N.4 was loaded into an ETH-type DAC (Miletich et al. 2000) using a steel gasket (T301), pre-indented to a thickness of 110 μ m and with a 250 μ m diameter hole. A single crystal of quartz was used as an internal diffraction pressure standard (Angel et al. 1997) with a hydrostatic pressure medium of 16:3:1 mixture of methanol:ethanol:water, which remains hydrostatic up to

TABLE 2. Unit-cell parameters at different pressure values for crystal N.4

P (GPa)	a (Å)	b (Å)	c (Å)	β (Å)	V (Å ³)
in air	9.5613(4)	8.7578(4)	5.2543(2)	106.953(1)	420.85(3)
0.0001(0)	9.568(1)	8.7608(15)	5.2561(8)	106.995(10)	421.36(9)
0.449(6)	9.5541(5)	8.7481(7)	5.2482(3)	106.895(4)	419.71(4)
1.245(8)	9.5346(5)	8.7292(7)	5.2376(4)	106.809(5)	417.30(4)
1.78(1)	9.5198(4)	8.715(1)	5.2296(6)	106.744(8)	415.48(7)
2.74(1)	9.4973(4)	8.6914(6)	5.2163(3)	106.630(4)	412.57(4)
3.41(1)	9.4810(5)	8.6745(6)	5.2078(3)	106.567(4)	410.52(4)
4.14(1)	9.4645(4)	8.6576(6)	5.1981(3)	106.497(4)	408.40(3)
5.02(1)	9.4452(6)	8.6368(9)	5.187(4)	106.412(6)	405.89(5)
5.89(1)	9.4278(6)	8.6165(7)	5.1769(4)	106.334(5)	403.57(4)
6.456(9)	9.4156(6)	8.6044(8)	5.1695(4)	106.228(5)	402.00(4)
7.11(2)	9.4030(5)	8.5913(7)	5.1620(3)	106.234(4)	400.37(4)
7.34(2)	9.3992(6)	8.5857(7)	5.1593(3)	106.216(5)	399.79(4)
7.55(2)	9.3949(6)	8.5832(9)	5.1574(5)	106.210(6)	399.35(5)

TABLE 3. Structure refinement details (the relative unit-cell parameters are reported in Table 2) for crystal N.4

P (GPa)	in air	0.0001	1.78	4.14	5.89	7.34
2 θ max (°)	78	60	60	60	60	60
R1 (%)	2.38	8.4	8.31	9.14	8.25	10.38
no. of $I/\sigma > 4$	2068	315	307	306	301	285
no. refl. tot.	2164	534	519	512	514	497
ref. param.	110	45	45	45	45	45
GoF	1.151	1.193	1.159	1.222	1.196	1.223
WR ² (%)	6.1	21.5	23.0	24.2	22.3	28.6

¹ Deposit item AM-12-011, CIFs. Deposit items are available two ways: For a paper copy contact the Business Office of the Mineralogical Society of America (see inside front cover of recent issue) for price information. For an electronic copy visit the MSA web site at <http://www.minsocam.org>, go to the *American Mineralogist* Contents, find the table of contents for the specific volume/issue wanted, and then click on the deposit link there.

TABLE 4. Site populations and degree of order of crystal N.4 in air

	Si	1.9639	M2	Ca	0.2531
	Al	0.0361		Na	0.7365
				Fe	0.0104
M1	Mg	0.8370			
	Fe	0.0921	M21	Ca	0.7128
	Al	0.0693		Na	0.2309
	Mn	0.0016		Mg	0.0563
M11	Mg	0.0157	Q ^{occ} _{M1}		0.8956
	Fe	0.0199			
	Al	0.9572	Q ^{occ} _{M2}		0.4993
	Ti	0.0058			
	Cr	0.0015	Q ^{dist} _{M1}		0.0689
			Q ^{dist} _{M2}		0.0161

TABLE 5. Fractional coordinates and displacement parameters for the crystal N.4

P (GPa)		in air	0.0001	1.77	4.14	5.89	7.34
M1	x	0.25	0.25	0.25	0.25	0.25	0.25
	y	0.15953(4)	0.1592(5)	0.1600(5)	0.1599(5)	0.1607(5)	0.1560(6)
	z	0.25	0.25	0.25	0.25	0.25	0.25
	U _{iso}	0.0069(1)	0.012(1)	0.012(1)	0.009(1)	0.009(1)	0.010(1)
M11	x	0.25	0.25	0.25	0.25	0.25	0.25
	y	0.34753(4)	0.3481(5)	0.3471(5)	0.3465(5)	0.3461(5)	0.3451(6)
	z	0.75	0.75	0.75	0.75	0.75	0.75
	U _{iso}	0.0058(1)	0.007(1)	0.008(1)	0.009(1)	0.009(1)	0.012(1)
M2	x	0.25	0.25	0.25	0.25	0.25	0.25
	y	0.55220(5)	0.5521(6)	0.5532(6)	0.5541(6)	0.5548(6)	0.5553(6)
	z	0.25	0.25	0.25	0.25	0.25	0.25
	U _{iso}	0.0103(1)	0.016(1)	0.014(1)	0.015(1)	0.014(1)	0.013(1)
M21	x	0.25	0.25	0.25	0.25	0.25	0.25
	y	0.95046(3)	0.9502(4)	0.9491(4)	0.9474(4)	0.9470(4)	0.9470(5)
	z	0.75	0.75	0.75	0.75	0.75	0.75
	U _{iso}	0.01079(9)	0.013(1)	0.013(1)	0.013(1)	0.012(1)	0.013(1)
Si1	x	0.53939(2)	0.5390(3)	0.5390(4)	0.5390(4)	0.5393(4)	0.5392(5)
	y	0.34783(2)	0.3485(3)	0.3493(3)	0.3484(4)	0.3490(3)	0.3495(4)
	z	0.22638(4)	0.2261(5)	0.2256(5)	0.2256(5)	0.2252(6)	0.2253(6)
	U _{iso}	0.00528(6)	0.0099(8)	0.0093(8)	0.0083(9)	0.0084(9)	0.010(1)
Si2	x	0.53731(2)	0.5368(3)	0.5378(4)	0.5376(4)	0.5375(4)	0.5378(5)
	y	0.16263(2)	0.1632(3)	0.1628(3)	0.1613(4)	0.1609(3)	0.1608(4)
	z	0.73036(4)	0.7307(5)	0.7308(5)	0.7303(5)	0.7291(6)	0.7293(6)
	U _{iso}	0.00510(6)	0.0086(8)	0.0085(8)	0.0084(9)	0.0095(9)	0.010(1)
O11	x	0.36286(6)	0.3626(8)	0.3631(8)	0.3627(9)	0.3616(9)	0.361(1)
	y	0.33887(7)	0.3358(8)	0.3374(8)	0.3390(8)	0.3398(7)	0.3392(8)
	z	0.1199(1)	0.118(1)	0.119(1)	0.122(1)	0.119(1)	0.120(1)
	U _{iso}	0.0075(1)	0.011(2)	0.011(2)	0.007(2)	0.007(2)	0.004(2)
O12	x	0.36109(6)	0.3623(7)	0.3618(8)	0.3606(9)	0.3610(9)	0.362(1)
	y	0.17821(7)	0.1769(8)	0.1762(8)	0.1758(8)	0.1749(9)	0.175(1)
	z	0.6483(1)	0.649(1)	0.650(1)	0.649(1)	0.650(1)	0.653(2)
	U _{iso}	0.0073(1)	0.010(2)	0.010(2)	0.011(2)	0.015(2)	0.016(2)
O21	x	0.61503(7)	0.6168(9)	0.6154(9)	0.6164(9)	0.6157(9)	0.617(1)
	y	0.51010(7)	0.5109(8)	0.5103(8)	0.5137(9)	0.5135(8)	0.517(1)
	z	0.3090(1)	0.310(1)	0.312(1)	0.312(1)	0.314(1)	0.315(1)
	U _{iso}	0.0086(1)	0.013(2)	0.013(2)	0.012(2)	0.012(2)	0.012(2)
O22	x	0.60598(7)	0.6050(8)	0.6051(9)	0.6054(9)	0.6061(9)	0.607(1)
	y	0.99774(7)	0.9984(8)	0.9975(8)	0.9944(8)	0.9941(8)	0.9926(9)
	z	0.8048(1)	0.804(1)	0.806(1)	0.809(1)	0.811(1)	0.813(1)
	U _{iso}	0.0097(1)	0.011(2)	0.011(2)	0.009(2)	0.010(2)	0.012(2)
O31	x	0.60675(6)	0.6069(8)	0.6079(8)	0.6072(8)	0.6071(9)	0.607(1)
	y	0.26646(7)	0.2662(8)	0.2683(8)	0.2693(8)	0.2712(8)	0.2719(9)
	z	0.0041(1)	0.004(1)	0.002(1)	0.000(1)	0.002(1)	0.003(1)
	U _{iso}	0.0075(1)	0.009(2)	0.010(2)	0.008(2)	0.010(2)	0.010(2)
O32	x	0.59781(6)	0.5970(8)	0.5995(8)	0.6004(9)	0.6010(9)	0.600(1)
	y	0.24041(7)	0.2387(8)	0.2379(8)	0.2356(8)	0.2345(8)	0.235(1)
	z	0.4972(1)	0.498(1)	0.495(1)	0.494(1)	0.492(1)	0.491(1)
	U _{iso}	0.0081(1)	0.011(2)	0.011(2)	0.009(2)	0.012(2)	0.013(2)

about 9.5–10 GPa (Angel et al. 2007). Unit-cell parameters were determined at 13 different pressures up to about 7.5 GPa using a STOE STADI-IV four-circle diffractometer (operating at 50 kV and 40 mA) automated by SINGLE software (Angel and Finger 2011). The unit-cell parameters were measured centering about 20 reflections for each high-pressure experiment. Full details of the instrument and the peak-centering algorithms are provided by

TABLE 6. Selected bond lengths (Å) and angles (°) in the space group *P2₁/n* structure for the sample studied in this work

P (GPa)	in air	0.0001	1.78	4.14	5.89	7.34
T1-O11	1.6178(6)	1.620(8)	1.609(8)	1.603(9)	1.612(9)	1.614(10)
T1-O21	1.5962(6)	1.606(8)	1.585(8)	1.612(8)	1.598(7)	1.618(9)
T1-O31	1.6510(6)	1.657(8)	1.654(8)	1.640(9)	1.630(9)	1.624(10)
T1-O32	1.6608(6)	1.675(6)	1.673(6)	1.666(7)	1.665(7)	1.652(8)
<T1-O>	1.631(30)	1.640(32)	1.630(40)	1.630(28)	1.626(29)	1.627(17)
V(Å ³)	2.210(2)	2.24(2)	2.20(2)	2.20(2)	2.19(2)	2.19(3)
TOE	1.0059	1.0077	1.0077	1.0064	1.0065	1.0066
TAV (°)	25.6262	34.1313	33.8249	28.2997	28.1005	27.9951
TILT (°)	3.50(2)	3.9(2)	3.2(2)	3.2(2)	3.0(2)	2.3(3)
T2-O12	1.6185(6)	1.603(8)	1.610(8)	1.612(9)	1.603(10)	1.593(11)
T2-O22	1.5873(7)	1.585(8)	1.580(8)	1.588(8)	1.584(7)	1.594(9)
T2-O31	1.6670(6)	1.663(6)	1.660(6)	1.658(7)	1.663(7)	1.652(8)
T2-O32	1.6471(6)	1.637(7)	1.644(8)	1.641(8)	1.635(8)	1.632(10)
<T2-O>	1.630(35)	1.622(35)	1.624(36)	1.625(31)	1.621(35)	1.618(29)
V(Å ³)	2.207(2)	2.18(2)	2.18(2)	2.19(2)	2.17(2)	2.16(3)
TOE	1.0051	1.0044	1.0041	1.0043	1.0046	1.0047
TAV (°)	21.556	18.5843	17.0801	18.0703	19.3477	19.9658
TILT (°)	1.92(2)	2.0(2)	1.6(2)	1.4(2)	1.3(2)	1.4(3)
M1-O11	2.1281(7)	2.144(8)	2.109(8)	2.094(9)	2.084(8)	2.073(9)
M1-O12	2.0587(6)	2.065(5)	2.061(5)	2.044(6)	2.045(7)	2.055(8)
M1-O22	2.0267(7)	2.036(9)	2.026(9)	1.998(9)	1.991(9)	1.968(10)
<M1-O>	2.071(46)	2.072(35)	2.065(37)	2.045(43)	2.040(42)	2.032(50)
V(Å ³)	11.603(7)	11.62(7)	11.51(7)	11.19(7)	11.10(8)	10.96(8)
TOE	1.0144	1.0139	1.0135	1.0134	1.0137	1.0143
TAV (°)	46.7793	46.1522	44.5324	43.4855	44.4995	45.5613
M11-O11	1.9299(6)	1.924(5)	1.920(5)	1.927(6)	1.906(6)	1.903(7)
M11-O12	1.9859(6)	2.004(8)	1.986(8)	1.967(8)	1.960(9)	1.944(10)
M11-O21	1.8840(6)	1.866(9)	1.878(9)	1.844(9)	1.848(9)	1.825(10)
<M11-O>	1.933(46)	1.931(62)	1.928(49)	1.913(56)	1.905(50)	1.891(54)
V(Å ³)	9.546(6)	9.51(6)	9.48(6)	9.24(7)	9.13(7)	8.93(7)
TOE	1.0066	1.0073	1.0065	1.0072	1.0067	1.0066
TAV (°)	21.3266	22.1401	20.631	22.0344	21.2417	20.2871
M2-O11	2.3564(7)	2.381(8)	2.365(8)	2.334(9)	2.323(8)	2.316(9)
M2-O21	2.3640(6)	2.358(6)	2.347(6)	2.343(6)	2.331(6)	2.326(7)
M2-O31	2.6919(7)	2.695(8)	2.649(8)	2.617(9)	2.586(9)	2.57(10)
M2-O32	2.4603(7)	2.475(8)	2.458(8)	2.454(8)	2.448(8)	2.441(9)
<M2-O>	2.47(14)	2.48(14)	2.45(13)	2.45(12)	2.42(11)	2.41(11)
V(Å ³)	24.63(1)	24.8(1)	24.2(1)	23.8(1)	23.4(1)	23.2(2)
M21-O12	2.3924(7)	2.390(8)	2.376(8)	2.366(8)	2.350(9)	2.34(10)
M21-O22	2.3866(7)	2.391(6)	2.380(6)	2.366(6)	2.351(6)	2.336(7)
M21-O31	2.4743(7)	2.471(7)	2.468(7)	2.457(7)	2.462(7)	2.468(9)
M21-O32	2.77506	2.773(8)	2.723(7)	2.672(8)	2.643(8)	2.64(10)
<M21-O>	2.51(17)	2.51(17)	2.49(15)	2.46(13)	2.45(13)	2.45(13)
V(Å ³)	25.92(1)	26.0(1)	25.4(1)	24.7(1)	24.4(1)	24.2(2)
O31-O32-O31	169.46(04)	168.7(4)	167.9(4)	166.9(4)	165.9(4)	166.0(5)
O21-O22-O21	63.19(01)	63.19(13)	63.24(14)	63.95(14)	64.01(13)	64.52(15)

Note: Bond length and volume data from IVTON program.

Angel (2000). During the centering procedure, the effects of crystal offsets and diffractometer aberrations were eliminated from refined peak positions by the eight-position centering method of King and Finger (1979). Unit-cell parameters, obtained by vector least-squares (Ralph and Finger 1982) are reported for each pressure step in Table 2. The intensity data were collected about every 2 GPa using a second STOE STADI-IV single-crystal diffractometer equipped with an Oxford Diffraction CCD detector located in the same department (graphite monochromated MoK α radiation). The intensity data were collected in the $5 \leq 2\theta \leq 60^\circ$ range using a 1° ω -scan and an exposure time of 60 s per frame. The sample detector distance was 60 mm. The program CrysAlis RED (Oxford Diffraction) was used to integrate the intensity data, applying the Lorentz-polarization correction. The ABSORB 6.0 (Angel 2004) program was adopted to correct for absorption and also to take into account the effect of gasket

shadowing (Angel 2000). The package SHELX-97 (Sheldrick 2008) was used for structure refinements, which were performed in space group $P2_1/n$, starting from the atom coordinates by Pavese et al. (2000). The atomic scattering curves were taken from the *International Tables for X-ray Crystallography* (Wilson 1995). Isotropic displacement parameters were considered for all atoms. For each high-pressure refinement the site occupancies were constrained to the values obtained from the refinement relative to the crystal in air (see Table 4). The values of the conventional agreement factor $R1$ as well as other details from every pressure step refinement are reported in Table 3. Fractional coordinates and displacement parameters are reported in Table 5, and bond lengths and angles in Table 6. The full structural data have also been deposited as CIFs¹.

RESULTS

Order degree

The site population (Table 4) was used to calculate the order parameters Q_{M1} and Q_{M2} of the M1 and M2 sites using Equations 2 and 3 provided by Carpenter et al. (1990), expressed as

$$Q_{M1}^{occ} = \frac{\left| \frac{(Al + Fe^{3+})_{M1} - (Al + Fe^{3+})_{M11}}{\sum (Al + Fe^{3+})} \right| + \left| \frac{(Mg + Fe^{2+})_{M1} - (Mg + Fe^{2+})_{M11}}{\sum (Mg + Fe^{2+})} \right|}{2} \quad (1)$$

and

$$Q_{M2}^{occ} = \frac{\left| \frac{Na_{M2} - Na_{M21}}{\sum Na} \right| + \left| \frac{Ca_{M2} - Ca_{M21}}{\sum Ca} \right|}{2}. \quad (2)$$

The resulting values of Q_{M1}^{occ} and Q_{M2}^{occ} were 0.896 and 0.499, respectively. These values are in agreement with those reported by Boffa Ballaran (1998) for the same 74AM33 sample. The order parameters expressed in terms of mean bond lengths were calculated using

$$Q_{M1}^{dist} = \frac{\left| \langle M1-O \rangle - \langle M11-O \rangle \right|}{\frac{1}{2} \langle M1-O \rangle + \langle M11-O \rangle} \quad (3)$$

and

$$Q_{M2}^{dist} = \frac{\left| \langle M2-O \rangle - \langle M21-O \rangle \right|}{\frac{1}{2} \langle M2-O \rangle + \langle M21-O \rangle} \quad (4)$$

provided by Carpenter et al. (1990), which yielded $Q_{M1}^{dist} = 0.0689$ and $Q_{M2}^{dist} = 0.0161$ (Table 4). The correlation between the two parameters confirms the low-aegirine content for the N.4 sample (see Fig. 2 by Carpenter et al. 1990).

Evolution of the unit-cell parameters with pressure and pressure-volume equation of state

The evolutions of the unit-cell parameters and unit-cell volume with pressure are shown in Figures 1a and 1b. A continuous decrease of a , b , c , β angle, and volume, V , was observed as a function of pressure with no evidence of a phase transition up

to the maximum pressure reached. The a , b , c lattice parameters decreased by about 1.8, 2.0, and 1.9% up to 7.5 GPa, respectively, β by 0.7% and unit-cell volume by about 5.2%.

To define the best equation of state that adequately describes the pressure-volume trend for the sample studied, an $F_E f_E$ plot was constructed following Angel (2000). The plot (Fig. 2) shows that the data lie on a positively inclined straight line, indicating that a Birch-Murnaghan equation of state truncated to the third order (BM3-EoS, Birch 1947) must be used to fit the experimental pressure-volume data. Thus, using EoS-FIT 5.2 software (Angel 2002) it was possible to refine simultaneously to a BM3 the volume V_0 , the bulk modulus K_{T0} , and its first pressure derivative K' obtaining the following coefficients: $V_0 = 421.43(4) \text{ \AA}^3$, $K_{T0} = 122(1) \text{ GPa}$, $K' = 5.1(3)$. The quality of the experimental data are demonstrated by the small differences between the EoS coefficients obtained by the refinement and by the $F_E f_E$ plot of Figure 2 [$K_{T0} = 122.9(6) \text{ GPa}$, $K' = 4.9(2)$]; the intercept corresponds to the bulk modulus, whereas the slope of the straight line provides the first pressure derivative as in Angel (2000).

A parameterized form of the BM3 EoS was used to determine the axial moduli of a , b , and c again using EoS-FIT5.2. Equation-of-state coefficients together with the relative axial compressibilities are reported in Table 7. The anisotropy scheme, using the data reported in Table 7, is $\beta_c \leq \beta_a \leq \beta_b$, with an anisotropy ratio 1.04:1.00:1.07.

Crystal-structure evolution with pressure

Figures 3 and 4 show the evolution of the polyhedral volumes for M1, M11, M2, and M21 sites as a function of pressure (data calculated using IVTON program, Balić-Žunić and Vicković 1996). For M2 and M21 polyhedra, we observed a continuous decrease of volume with pressure by about 6.4 and 6.9%, respectively (Fig. 4). A large deformation can be seen in the M2 polyhedron: the M2-O31 bond length shows a strong decrease of close to 4.5% (see Table 6); for the M21 polyhedron the M21-O32 bond length decreases even more, with a reduction of about 5.7% (see Table 6). This striking difference could explain the slightly greater volumetric reduction of the M21 polyhedron.

The M1 and M11 polyhedra show a smaller decrease in volume (of about 5.7 and 6.1%, respectively) than M2 sites. The M11 polyhedron is slightly softer than M1 and this is likely due to the greater compressibility of the two bond lengths M1-O11 and M1-O22, which show a decrease of 2 and 3.3%, respectively, against M11-O21 and M11-O12 bond lengths, which decrease by 1.2 and 3%, respectively (see Table 6). In Figures 3 and 4, it is possible to note that both M1 and M2 polyhedra show a slight but significant change in slope at about 4 GPa. This behavior cannot be explained in terms of bond length compression anomaly but more likely by the tilt angle [defined as the out-of-plane tilting of the basal face of the tetrahedral with respect to the plane (100) (see Cameron et al. 1973)] variation as a function of pressure. Indeed, in Figure 5 the tilt angles of both TA and TB show a slope change between 2 and 4 GPa.

The TA and TB tetrahedra show a small decrease in volume up to the maximum pressure reached during the experiments, as usually expected for such very rigid polyhedra as a function of pressure. However, a slight difference in compressibility between TA and TB was found (2.2 and 0.9%, respectively, up to 7.3 GPa).

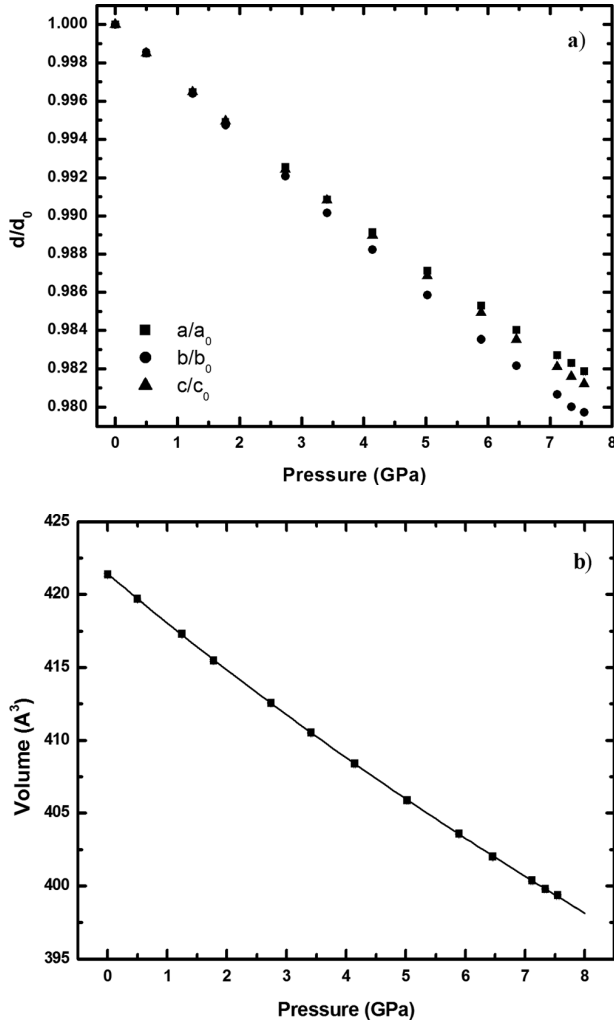


FIGURE 1. Evolution of the (a) unit-cell parameters and (b) unit-cell volume as a function of pressure for all the samples investigated. The symbols used are larger than the errors. The curve plotted in **b** is the real equation of state for the sample.

The O3-O3-O3 angle, defining the tetrahedral chain kinking, decreases linearly by about 1.7% up to 6 GPa and then remained constant up to the maximum pressure reached.

DISCUSSION AND CONCLUDING REMARKS

The K_{T0} value of our sample, obtained using a BM3-EoS, was plotted vs. composition expressed in molar percentage of jadeite in Figure 6. In this figure, the value for pure jadeite is from Nestola et al. (2006), very close to McCarty et al.'s (2008) value. We decided to use Nestola et al.'s (2006) data because they were obtained using the same experimental techniques as those used in this work. The diopside value is from Gavrilenko et al. (2010). Their data are the most recent on diopside compressibility and were calculated with the same experimental techniques used in this work, and in Nestola et al. (2006), using a BM3-EoS to obtain the bulk modulus. Gavrilenko et al. (2010) investigated two diopside samples: a first sample, Di_{anhyd} (named Di_0) with

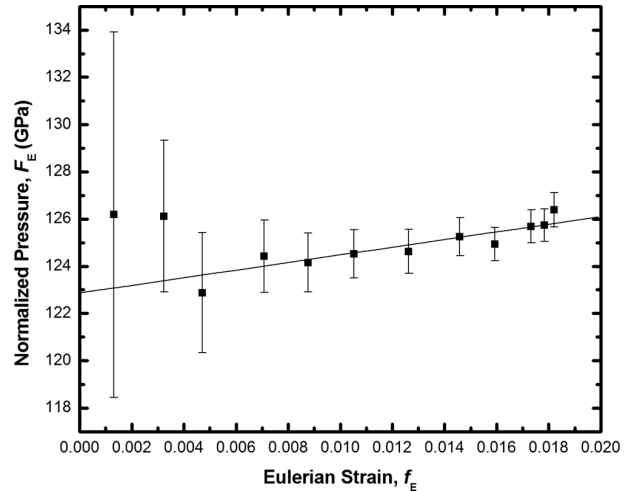


FIGURE 2. $F_E - f_E$ plot $\{F_E = P/3 \times f_E \times (1 + 2f_E)/5$ and $f_E = [(V_0/V)^{2/3} - 1]/2$, see Angel 2000} for the sample studied in this work.

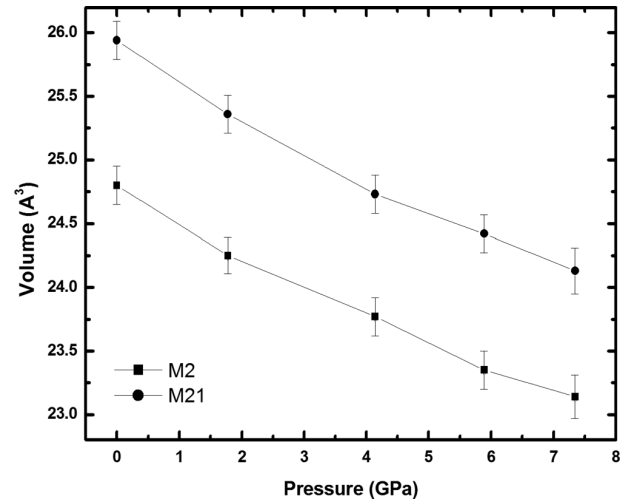


FIGURE 3. Evolution of M1 polyhedral volumes as a function of pressure.

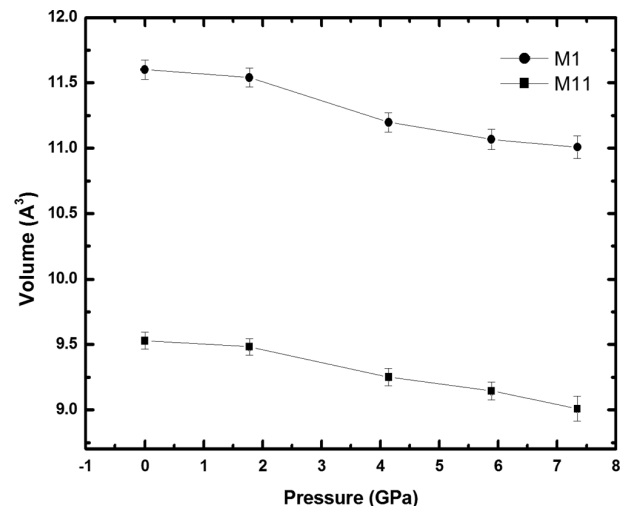


FIGURE 4. Evolution of M2 polyhedral volumes as a function of pressure.

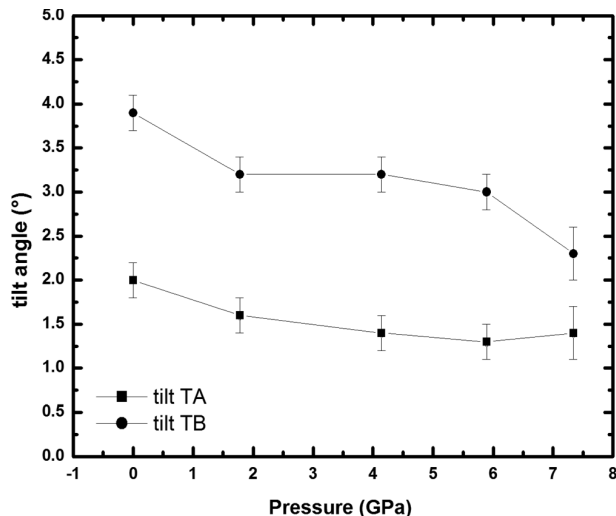


FIGURE 5. Evolution of the tilt angle as a function of pressure for the two tetrahedral chains TA and TB.

TABLE 7. Equation of state coefficients for N.4 using a third-order Birch-Murnaghan equation

a_0	9.5685(5)	b_0	8.7618(7)	c_0	5.2558(3)	V_0	421.43(4)
Ka_0	112(2)	Kb_0	107(2)	Kc_0	115(2)	K_{T0}	122(1)
K'	7.6(5)	K'	3.9(5)	K'	4.9(5)	K'	5.1(3)

K_{T0} (GPa) = 106(1) does not have a pure diopside composition (i.e., a limited excess of Mg), whereas a second sample, Di_{hyd} (named Di_{600}) with K_{T0} (GPa) = 108(1), is hydrated (e.g., 600 ppm). However, it clearly appears that, despite their non purity, neither sample shows any significant bulk modulus deviation from the synthetic diopside reported by Tribaudino et al. (2000), K_{T0} (GPa) = 105.1(9), from the value of K_{T0} (GPa) = 108 GPa computed from the adiabatic bulk modulus reported by Levien et al. (1979), or from the value extrapolated by Boffa Ballaran et al. (2009) on a pure diopside sample, K_{T0} (GPa) = 107.4(1).

In Figure 6, the data referring to $Jd_{100}Di_0$ (Nestola et al. 2006), $Jd_{35}Di_{45}$ (our sample N.4), and Jd_0Di_{100} (Gavrilenco et al. 2010) lie on a well-defined bulk modulus vs. composition trend, which shows a clear curvature at intermediate composition. Along the jadeite-diopside solid solution the bulk modulus K_{T0} decreases by about 9% from 134.0(7) GPa for jadeite to the value of 122(1) GPa for our sample, down to 106(1) GPa for diopside with a total decrease of about 21%. The value of the bulk modulus from Pavese et al. (2001) lies very close to the trend in Figure 6.

Figure 6 also reports the data from Nishihara et al. (2003), K_{T0} (GPa) = 126(1); and from samples SBB-1, K_{T0} (GPa) = 129(3) and SDC-1 K_{T0} (GPa) = 139(4) by McCormick et al. (1989). None of these data correspond strictly to $Jd_{50}Di_{50}$ composition and were all calculated using a BM2-EoS with K' assumed to be 4. The recalculation of the data, using a BM3-EoS for purpose of comparison with our data, led to a negative K' value. In addition, the SBB-1 sample by McCormick et al. (1989); and the sample by Nishihara et al. (2003) contain 13 and 9% of Ca-Eskola ($Ca_{0.5}Al_{0.5}Si_2O_6$, vacancy-rich end-member), respectively. Finally, as already observed by McCormick et al. (1989) themselves, "there is a significant difference in the compression of the two omphacites, with the vacancy-rich pyroxene (SBB-1) being

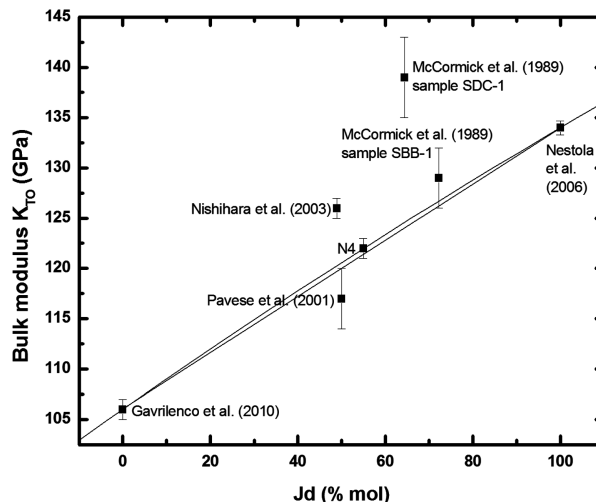


FIGURE 6. Evolution of K_{T0} as a function of composition along the diopside-jadeite join.

more compressible than the vacancy-poor pyroxene (SDC-1)." At any rate, the effect on the compressibility of the presence of Ca-Ts ($CaAl_2Si_2O_6$ end-member) cannot be neglected: and the samples that deviate more from the trend are those containing the greatest percentage of Ca-Ts: 6.2 and 4.6%, respectively, for SDC-1 and for Nishihara et al.'s (2003) samples. The influence of tetrahedral Al on the bulk modulus had already been highlighted by Nestola et al. (2008b) for an aluminum-rich orthopyroxene sample, where significant stiffening was reported.

Concerning the first pressure derivative, K' , it increases nearly linearly as a function of the diopside content from 4.4(1) for jadeite (Nestola et al. 2006) to 5.1(3) (our study) to 6.1(5) for pure diopside (Gavrilenco et al. 2010) as found for the jadeite-hedenbergite join (Nestola et al. 2008a). It is well known (see Angel 2000) that there is a correlation of about 95% between the bulk modulus and its first pressure derivative. The strength of this correlation often covers the real errors in determining both parameters, as during the least-squares refinement they are considered as two independent parameters. In this light, to better understand the K_{T0} - K' correlation along the Jd-Di join, a series of confidence ellipses in the parameter space was constructed following Angel (2000). The confidence ellipse, shown in Figure 7, was calculated for our sample, as well as for diopside (Gavrilenco et al. 2010), omphacite (Pavese et al. 2001), and jadeite (Nestola et al. 2006) up to a confidence level of 68.3%. In this figure, a negative correlation can be seen for all four samples. Considering the extension of the ellipses, the errors on K_{T0} and K' must be reconsidered for all of them: for jadeite (Nestola et al. 2006), the errors on K_{T0} and K' increase only slightly from 0.7 GPa and 0.1 to 1 GPa and 0.3, respectively; for diopside (Gavrilenco et al. 2010), the errors on K_{T0} and K' increase from 1 GPa and 0.5 to 2 GPa and 0.7, respectively; for our omphacite sample, the errors on K_{T0} and K' increase from 1 GPa and 0.3 to 2 GPa and 0.5, respectively; finally for the omphacite samples by Pavese et al. (2001), the errors increase from 2.5 GPa and 0.6 to 4 GPa and 1.0, respectively, suggesting that some non hydrostaticity could be the cause of this substantial increase in K_{T0} and K' errors

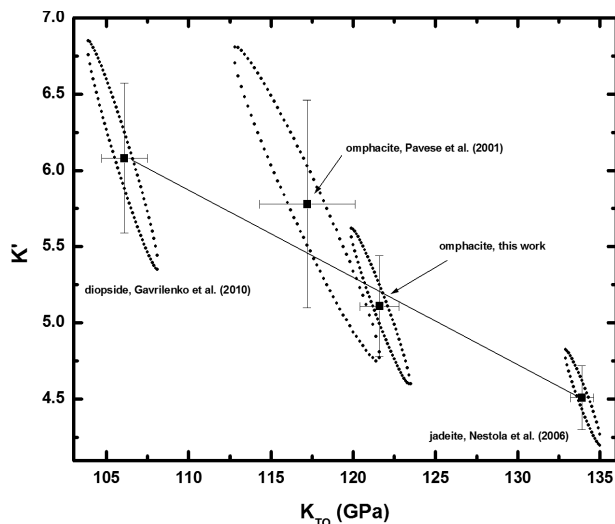


FIGURE 7. Confidence ellipse for the equation of state of the sample studied in this work and for other samples studied along the diopside-jadeite join.

due to their correlation. In support of this explanation, Pavese et al. (2001) obtained their EoS by X-ray powder diffraction up to 13 GPa using synchrotron radiation with nitrogen as a pressure medium. As demonstrated by Angel et al. (2007), nitrogen is a non-hydrostatic pressure medium for pressures above 2–3 GPa.

To explain the difference in compressibility along the jadeite-diopside solid solution, the structural deformation mechanisms along the join have to be taken into account. Thompson and Downs (2008) and Nestola et al. (2008a) described the main three deformation mechanisms: isotropic scaling of the structure, tetrahedral chain kinking and narrowing of the M1 chain along the **b** direction. For our omphacite sample, we observed the following high-pressure behavior: (1) the axial bulk modulus anisotropy is relatively limited with differences lower than 7% (Table 7); (2) the tetrahedral chain shows a significant contraction of about 0.47°/GPa, thus affecting the M2-O31 bond length, which shows the strongest contraction (about 0.017 Å/GPa) compared with the other bond lengths; and (3) the angle between O21-O22-O21, which can be used as an indication of the narrowing of the M1 chain (see Fig. 8), increases by 1.3° up to 7.34 GPa (Table 6).

To verify whether we could find any systematic structural deformation mechanism along the diopside-jadeite join we compared our sample with the two end-members: diopside and jadeite (Thompson and Downs 2008; Nestola et al. 2008a). In particular, in terms of contraction of the tetrahedral chain and M1 chain narrowing, we did not find a significantly different behavior of our sample compared to that of the end-members.

Taking into account the linear compressibility {expressed as $\beta = [(V - V_0)/V_0]/\Delta P$ } of the structural M1 and M2 polyhedra, a possible comparison of our space group *P2/n* omphacite with the two end-members can be performed on the basis of the site population of the structural sites. Regarding the M1 polyhedra, in an ordered space group *P2/n* omphacite, the M11 of omphacite is similar to the M1 of jadeite due to its aluminum content ($X_{M11}^{Al} = 0.957$) while because of its Mg content ($X_{M1}^{Mg} = 0.837$), M1 is similar to the M1 of diopside. Concerning M2 polyhedra, the comparison

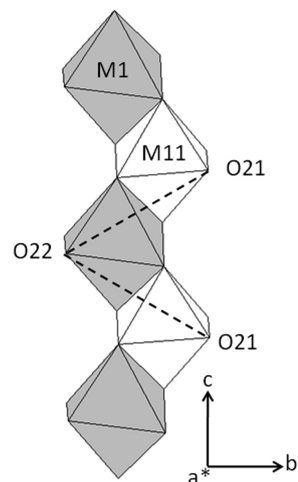


FIGURE 8. Part of the crystal-structure of the sample studied in this work viewed along the [100] direction. The octahedral M1 and M11 sites are shown. The black line corresponds to the O21-O22-O21 angle.

of the M2 polyhedron in omphacite with the correspondent M2 of jadeite and the M21 polyhedron to the corresponding M2 of diopside is more questionable due to the partial order of Na and Ca. The linear compressibility of the M2 polyhedron of omphacite shows a similar value to that of the M2 polyhedron of jadeite ($\beta_{M2} = 0.0088$ and $\beta_{M2} = 0.0090$ GPa⁻¹, respectively), whereas the linear compressibility of its M11 polyhedron is greater than that of the correspondent in jadeite (β_{M11} of omphacite = 0.0083 GPa⁻¹, β_{M11} of jadeite = 0.0065 GPa⁻¹). This supports the evidence for a lower bulk modulus for the space group *P2/n* omphacite (K_{T0} omphacite is 122 GPa with respect to the K_{T0} of 134 GPa for jadeite). However, similar relationships have not been found in comparisons between omphacite and diopside. Indeed, whereas the linear compressibility of the M1 polyhedron is identical for both clinopyroxenes ($\beta_{M1} = 0.0077$ GPa⁻¹), the value of the M21 polyhedron of omphacite is significantly greater than that of the M2 polyhedron of diopside ($\beta_{M21} = 0.0094$ and $\beta_{M2} = 0.0080$ GPa⁻¹, respectively). This is in contrast with the evidence for a greater bulk modulus for the space group *P2/n* omphacite with respect to diopside ($K_{T0} = 106$).

If the variation in the M1 and M2 polyhedral volumes with pressure (Figs. 3 and 4) is considered in detail, a linear fit can be used. Concerning M1, the coefficient describing the slope of the straight line confirms the similarity of the behavior of the M11 polyhedron of omphacite with the M1 polyhedron of jadeite [0.079(9) vs. 0.061(8), respectively] and of the M1 polyhedron of omphacite and diopside [0.093(7) vs. 0.091(2), respectively]. For M2, the same coefficient does confirm the similarity between the M2 polyhedra of omphacite and jadeite [0.22(2) vs. 0.22(3), respectively] but shows the same contrast between the M21 polyhedron of omphacite and the M2 polyhedron of diopside [0.25(2) vs. 0.205(7), respectively] already observed above.

It appears that while about 25% of the Ca in M2 of omphacite does not affect the compressibility of this polyhedron with respect to that of jadeite, the same amount of Na in the M21 polyhedron of omphacite increases the compressibility of this polyhedron

with respect to that of the M2 polyhedron of diopside. It is remarkable that the averaged effect of the various polyhedra is indeed intermediate between those of Jd and Di (reported also in Figs. 3 and 4), as it is for the bulk modulus.

ACKNOWLEDGMENTS

This work was funded by F.A.R., University of Pavia. We thank Roberto Gastoni CNR-Pavia for sample preparation for EMPA analyses and R. Carampin of CNR-Padova for the use of WDS electron microprobe facilities. We thank Jennifer Kung, Associate Editor of *American Mineralogist*, Ron Peterson, and two anonymous reviewers for their comments on this paper.

REFERENCES CITED

- Agee, C.B. (1999) Phase transformations and seismic structure in the upper mantle and transition zone. In R.J. Hemley, Ed., *Ultrahigh-pressure Mineralogy: Physics and Chemistry of the Earth's Deep Interior*, 37, p. 165–203. *Reviews in Mineralogy and Geochemistry*, Mineralogical Society of America, Chantilly, Virginia.
- Angel, R.J. (2000) Equations of State. In R.M. Hazen and R.T. Downs, Eds., *High-Temperature and High-Pressure Crystal Chemistry*, 41, p. 35–39. *Reviews in Mineralogy and Geochemistry*, Mineralogical Society of America, Chantilly, Virginia.
- (2002) EOSFIT V5.2 program. Crystallography Laboratory, Virginia Tech, Blacksburg, Virginia.
- (2004) Absorption corrections for diamond-anvil cells implemented in the software package Absorb 6.0. *Journal of Applied Crystallography*, 37, 486–492.
- Angel, R.J. and Finger, L.W. (2011) SINGLE: a program to control single-crystal diffractometers. *Journal of Applied Crystallography*, 44, 247–251.
- Angel, R.J., Allan, D.R., Miletich, R., and Finger, L.W. (1997) The use of quartz as an internal pressure standard in high pressure crystallography. *Journal of Applied Crystallography*, 30, 461–466.
- Angel, R.J., Bujak, M., Zhao, J., Gatta, D., and Jacobsen, S.D. (2007) Effective hydrostatic limits of pressure media for high-pressure crystallographic studies. *Journal of Applied Crystallography*, 40, 26–32.
- Balić-Zunić, T. and Vicković, I. (1996) IVTON-program for the calculation of geometrical aspects of crystal structures and some crystal chemical applications. *Journal of Applied Crystallography*, 29, 305–306.
- Bindi, L., Downs, R.T., Harlow, G.E., Safonov, O.G., Litvin, Y.A., Perchuk, L.L., Uchida, H., and Menchetti, S. (2006) Compressibility of synthetic potassium-rich clinopyroxene: In-situ high-pressure single-crystal X-ray study. *American Mineralogist*, 91, 802–808.
- Birch, F. (1947) Finite elastic strain of cubic crystals. *Physical Review*, 71, 809–824.
- Blessing, R.H. (1995) An empirical correction for absorption anisotropy. *Acta Crystallographica*, 51, 33–38.
- Boffa Ballaran, T., Carpenter, M.A., Domeneghetti, M.C., and Tazzoli, V. (1998) Structural mechanisms of solid solution and cation ordering in augite-jadeite pyroxenes: I. A macroscopic perspective. *American Mineralogist*, 83, 419–433.
- Boffa Ballaran, T., Nestola, F., Tribaudino, M., and Ohashi, H. (2009) Bulk modulus variation along the diopside–kosmochlor solid solution. *European Journal of Mineralogy*, 21, 591–597.
- Cameron, M., Sueno, S., Prewitt, C.T., and Papike, J.J. (1973) High temperature crystal chemistry of acmite, diopside, hedenbergite, jadeite, spodumene, and ureyite. *American Mineralogist*, 58, 594–618.
- Carpenter, M.A., Domeneghetti, M.C., and Tazzoli, V. (1990) Application of Landau theory to cation ordering in omphacite I: Equilibrium behavior. *European Journal of Mineralogy*, 2, 7–18.
- Downs, R.T. (2003) Topology of the pyroxenes as a function of temperature, pressure, and composition as determined from the procrystal electron density. *American Mineralogist*, 88, 556–566.
- Gavrilenko, P., Boffa Ballaran, T., and Kepler, H. (2010) The effect of Al and water on the compressibility of diopside. *American Mineralogist*, 95, 608–616.
- Hawthorne, F.C., Ungaretti, L., and Oberti, R. (1995) Site populations in minerals: terminology and presentation of results of crystal-structure refinement. *Canadian Mineralogist*, 33, 907–911.
- King, H.E. and Finger, L.W. (1979) Diffracted beam crystal centering and its application to high-pressure crystallography. *Journal of Applied Crystallography*, 12, 374–378.
- Koch-Müller, M., Matsyuk, S.S., and Wirth, R. (2004) Hydroxyl in omphacites and omphacitic clinopyroxenes of upper mantle to lower crustal origin beneath the Siberian platform. *American Mineralogist*, 89, 921–931.
- Levien, L., Weidner, D.J., and Prewitt, C.T. (1979) Elasticity of diopside. *Physics and Chemistry of Minerals*, 4, 105–113.
- McCarty, A.C., Downs, R.T., and Thompson, R.M. (2008) Compressibility trends of the clinopyroxenes, and in-situ high-pressure single-crystal X-ray diffraction study of jadeite. *American Mineralogist*, 93, 198–209.
- McCormick, T.C., Hazen, R.M., and Angel, R.J. (1989) Compressibility of omphacite to 60 kbar: Role of vacancies. *American Mineralogist*, 74, 1287–1292.
- Miletich, R., Allan, D.R., and Kuhs, W.F. (2000) High-pressure single-crystal techniques. In R.M. Hazen and R.T. Downs, Eds., *High-Temperature and High-Pressure Crystal Chemistry*, 41, p. 445–519. *Reviews in Mineralogy and Geochemistry*, Mineralogical Society of America, Chantilly, Virginia.
- Nestola, F., Ballaran, T.B., Tribaudino, M., and Ohashi, H. (2005) Compressional behaviour of CaNiSi₂O₆ clinopyroxene: bulk modulus systematic and cation type in clinopyroxenes. *Physics and Chemistry of Minerals*, 32, 222–227.
- Nestola, F., Boffa Ballaran, T., Liebske, C., Bruno, M., and Tribaudino, M. (2006) High-pressure behaviour along the jadeite NaAlSi₃O₆–aegirine NaFeSi₃O₆ solid solution up to 10 GPa. *Physics and Chemistry of Minerals*, 33, 417–425.
- Nestola, F., Tribaudino, M., Boffa Ballaran, T., Liebske, C., and Bruno, M. (2007) The crystal structure of pyroxenes along the jadeite–hedenbergite and jadeite–aegirine joins. *American Mineralogist*, 92, 1492–1501.
- Nestola, F., Boffa Ballaran, T., Liebske, C., Thompson, R., and Downs R.T. (2008a) The effect of the hedenbergitic substitution on the compressibility of jadeite. *American Mineralogist*, 93, 1005–1013.
- Nestola, F., Boffa Ballaran, T., and Balić-Zunić, T. (2008b) The high-pressure behavior of an Al- and Fe-rich natural orthopyroxene. *American Mineralogist*, 93, 644–652.
- Nestola, F., Boffa Ballaran, T., Angel, R.J., Zhao, J., and Ohashi, H. (2010) High-pressure behaviour of Ca/Na clinopyroxenes: The effect of divalent and trivalent 3d-transition elements. *American Mineralogist*, 95, 832–838.
- Nishihara, Y., Takahashi, E., Matsukage, K., and Kikegawa, T. (2003) Thermal equation of state of omphacite. *American Mineralogist*, 88, 80–86.
- Origlieri, M.J., Downs, R.T., Thompson, R.M., Pommier, C.J.S., Denton, M.B., and Harlow, G.E. (2003) High-pressure crystal structure of kosmochlor NaCrSi₃O₆ and systematics of anisotropic compression in pyroxenes. *American Mineralogist*, 88, 1025–1032 and 1632.
- Pavese, A., Bocchio, R., and Ivaldi, G. (2000) In situ high temperature single crystal X-ray diffraction study of a natural omphacite. *Mineralogical Magazine*, 64, 983–993.
- Pavese, A., Diella, V., Devy, D., and Hanfland, M. (2001) Synchrotron X-ray diffraction study of a natural *P2₁/n* omphacites at high pressure conditions. *Physics and Chemistry of Minerals*, 28, 9–16.
- Pouchou J.L. and Pichoir F. (1991) Quantitative analysis of homogeneous or stratified microvolumes applying the model “PAP.” In K.F.J. Heinrich and D.E. Newbury, Eds., *Electron Probe Quantization*, p. 31–75. Plenum Press, New York.
- Ralph, R.L. and Finger, L.W. (1982) A computer program for refinement of crystal orientation matrix and lattice constraints from diffractometer data with lattice symmetry constraints. *Journal of Applied Crystallography*, 15, 537–539.
- Sheldrick, G.M. (1996) SADABS. University of Göttingen, Germany.
- (2008) A short history of SHELX. *Acta Crystallographica*, A64, 112–122.
- Tribaudino, M., Principe, M., Bruno, M., and Levy, D. (2000) High-pressure behavior of Ca-rich *C2/c* clinopyroxenes along the join diopside–enstatite (CaMgSi₂O₆–Mg₂Si₂O₆). *Physics and Chemistry of Minerals*, 27, 656–664.
- Thompson, R.M. and Downs, R.B. (2008) The crystal structure of diopside at pressure to 10 GPa. *American Mineralogist*, 93, 177–186.
- Thompson, R.M., Downs, R.T., and Redhammer, G.J. (2005) Model pyroxenes III: Volume of *C2/c* pyroxenes at mantle *P*, *T*, and *x*. *American Mineralogist*, 90, 1840–1851.
- Wilson, A.J.C. (1995) *International Tables for Crystallography*. Volume C. Kluwer Academic Publishers, Dordrecht.
- Zema, M., Domeneghetti, M.C., Molin, G.M., and Tazzoli, V. (1997) Cooling rates of diogenites: A study of Fe²⁺–Mg ordering in orthopyroxene by single-crystal X-ray diffraction. *Meteoritics and Planetary Science*, 32, 855–862.

MANUSCRIPT RECEIVED JUNE 28, 2011

MANUSCRIPT ACCEPTED OCTOBER 17, 2011

MANUSCRIPT HANDLED BY JENNIFER KUNG